The effects of local graphitization on the charging mechanisms of microporous carbon supercapacitor electrodes

Huan Yin, Hui Shao, Barbara Daffos, Pierre-Louis Taberna, Patrice Simon

Electrochemistry Communications 137 (2022) 107258

Contents lists available at ScienceDirect

Electrochemistry Communications

journal homepage: www.elsevier.com/locate/elecom

Full Communication

The effects of local graphitization on the charging mechanisms of microporous carbon supercapacitor electrodes

Huan Yin [a,b], Hui Shao [a,b], Barbara Daffos [a,b], Pierre-Louis Taberna [a,b,*], Patrice Simon [a,b,*]

[a] Université Paul Sabatier, CIRIMAT UMR CNRS 5085, 118 Route de Narbonne, 31062 Toulouse, France
[b] Réseau sur le Stockage Electrochimique de l'Energie (RS2E), FR CNRS 3459, France

ARTICLE INFO

Keywords:
Electrical double-layer capacitance
Nanoporous carbon
Charge storage mechanism
Electrochemical quartz crystal microbalance

ABSTRACT

The electrochemical quartz crystal microbalance (EQCM) technique has been used to study the charge mechanisms in two TiC-derived nanoporous carbons (CDC), synthesized at 800 °C and 1100 °C. These two carbons have a similar pore size and porous volume, but the CDC prepared at 1100 °C shows a more graphitic microstructure. The EQCM study revealed that the charge storage mechanism in the CDC-800 is mainly controlled by a counter-ion adsorption process, while an expanded ion-exchange process was observed for the CDC-1100. Combined with the potential of zero charge (PZC), these measurements suggest a strong interaction between the anions and graphitic carbon. For the first time, we provide experimental evidence that the local carbon structure affects the charge storage mechanism of the electrical double-layer capacitance in high surface area porous carbons.

1. Introduction

Electrochemical double-layer capacitors (EDLCs), also known as supercapacitors, exhibit a high power density suitable for a broad range of applications where high power delivery or uptake is needed [1,2]. The charge storage mechanism in EDLCs is based on the reversible physical adsorption of ions at the electrode/electrolyte interface of porous carbons with a high surface area [3,4].

Porous carbons are widely used as electrode materials for EDLCs due to their excellent electrical conductivity and high specific surface area (SSA) [5]. Titanium-carbide-derived carbons (TiC-CDCs) are porous carbons with a narrow pore size distribution and a tunable pore structure and size, obtained by selective etching of Ti atoms through chlorine treatment at a temperature > 400 °C [6,7]. Nanoporous TiC-CDCs with pore sizes in the 0.6–1.2 nm range with a high specific surface area (up to 1700 $m^2 \cdot g^{-1}$) and a large pore volume (up to 1.6 $cm^3 \cdot g^{-1}$) can be prepared, resulting in an impressive specific capacitance, thanks to the discovery of the confinement effect and the associated ion partial desolvation in the nanopores [1,2,8,9]. Since that time, tremendous efforts have been focused on understanding the charge storage mechanisms in porous carbon electrodes, especially the ion fluxes in confined nanopores [1,10,11] which affect the ion population inside the pores and the charging rate [12,13]. Previous studies have suggested three main charge mechanisms in EDLCs, as the result of the ion dynamics occurring at the electrode/electrolyte interface with (i) counter-ion adsorption, (ii) ion exchange, and (iii) a co-ion desorption process [13,14]. However, how the local carbon structure affects the charging mechanisms still remains poorly understood.

Recently, we studied the electrical double-layer (EDL) charge storage mechanism of two-dimensional (2D), singlelayer graphene (SLG) used as a model material in both neat ionic liquid and solvated electrolyte, with the help of the electrochemical quartz crystal microbalance (EQCM) technique. We found that the EDL charging mechanisms are highly dependent on the interactions between ions and carbon [15,16]. However, the situation is much more complex in 3D porous carbon, and there has been no work about how the local structure of three-dimensional carbon affects the charging mechanisms, apart from modeling studies [17]. As previous work has demonstrated that the local structures of TiC-CDCs are highly dependent on the synthesis temperature, such materials represent a suitable platform for obtaining experimental data regarding the influence of the local structure on the charging mechanism. TiC-CDCs prepared at temperatures less than 700 °C mainly possess a disordered microstructure. Short-range structural ordering starts to appear in TiC-CDCs prepared at temperatures in the range 800–1000 °C, while longer-range structural ordering (graphitization) occurs when the synthesis temperature is higher than 1100 °C [18,19]. It is worth noting that the porosities of the TiC-CDCs prepared at 800 °C (CDC-800) and 1100 °C (CDC-1100) are similar [6]. Therefore, we selected these two

* Corresponding authors.
E-mail addresses: pierre-louis.taberna@univ-tlse3.fr (P.-L. Taberna), patrice.simon@univ-tlse3.fr (P. Simon).

https://doi.org/10.1016/j.elecom.2022.107258
Received 18 January 2022; Received in revised form 26 February 2022; Accepted 2 March 2022
Available online 4 March 2022

TiC-CDCs prepared at 800 °C and 1100 °C (denoted CDC-800 and CDC-1000, respectively), with similar porous volumes and pore sizes but different degrees of graphitization – so different local structures – to explore ion dynamics in a non-aqueous electrolyte by EQCM. A comparison between these two CDCs should lead to a better understanding of the carbon local structure–ion dynamics correlation in porous carbon.

2. Experimental

Samples of CDC-800 and CDC-1100 were prepared by chlorination of the carbides for 3 h at temperatures of 800 ℃ and 1100 ℃, respectively [6]. The structure and properties of CDC-800 and CDC-1100 were characterized by transmission electron microscopy (TEM, JEOL 2100F) and Ar sorption measurements conducted at 77 K. The pore size distribution (PSD) was calculated from adsorption isotherms using a 2D non-local density functional theory (2D-NLDFT) model based on Saeius software from Micromeritics Equipment. Homogenous slurries of 90 wt % carbon material and 10 wt% polyvinylidene fluoride (PVDF) binder in *N*-methyl-2-pyrrolidone (NMP) were prepared and spray-coated onto 1-inch-diameter Au-coated AT-cut quartz crystals (AWSensors, 1.28 cm^2). The coated quartz crystals were dried overnight in a vacuum oven at 80 °C. The loading mass of TiC-CDC was maintained at around 30 to 40 $\mu g \cdot cm^{-2}$ to stay within the linear region of the Sauerbrey equation (eqn. (1)). The electrochemical cell was assembled in a glove box under argon using the coated quartz crystal, a silver rod and a platinum foil as the working, reference and counter electrode, respectively. EQCM electrochemical measurements were conducted using a Seiko QCM system combined with a SP-200 potentiostat in 2 M 1-ethyl-3-methylimidazolium bis(trifluoromethane-sulfonyl)imide (EMI-TFSI) in acetonitrile (ACN) electrolyte. The PZC value was determined by the minimum capacitance from cyclic voltammetry (CV) tests achieved in a three-electrode Swagelok cell, utilizing a TiC-CDC working electrode (0.8 to 1.3 $mg \cdot cm^{-2}$), a silver rod reference electrode and an over capacitive counter electrode carbon film (25 $mg \cdot cm^{-2}$), obtaining by mixing YP50F activated porous carbon powder (95 wt%) and poly-tetrafluoroethylene (5 wt%) solution. To calculate the electrode mass change during reactions, we used the Sauerbrey equation [20]:.

$$\Delta m = -\frac{A\sqrt{\rho_q \mu_q}}{2f_0^2} \bullet \Delta f = -C_f \bullet \Delta f \quad (1)$$

where Δm is electrode weight change per unit mass of carbon ($ng \cdot ng^{-1}$), A is the piezoelectrically active area (cm^2),ρ_q is the density of quartz (2.648 $g \cdot cm^{-3}$), μ_q is the shear modulus of quartz (2.947×10^{11} $g \cdot cm^{-1} \cdot s^{-2}$), f_0 is the fundamental resonance frequency of the quartz, C_f is the sensitivity factor of the quartz crystal (6.69 $ng \cdot Hz^{-1}$) and Δf_{exp} is the experimental frequency change (Hz). The frequency change was normalized with respect to the effective mass (M_{eff}, in ng), according to eqns. (2) and (3):

$$M_{eff(ng)} = \frac{C_{pzc,EQCM}(F)}{C_{pzc,swagelok}(F \cdot ng^{-1})} \quad (2)$$

$$\Delta f = \frac{\Delta f_{exp}}{M_{eff(ng)}} \quad (3)$$

where Δf is the normalized frequency change ($Hz \cdot ng^{-1}$);$C_{pzc,EQCM}$, the capacitance measured from the EQCM cell at the PZC (F) and$C_{pzc,swagelok}$, the capacitance measured from the Swagelok cell at the PZC ($F \cdot ng^{-1}$).

The theoretical mass change of bare ions (m) was calculated from Faraday's law:.

$$m = \frac{Q \bullet M_w}{n \bullet F} = \frac{I \bullet t \bullet M_w}{n \bullet F} \quad (4)$$

where Q is the charge passed through the electrode (C), M_w is the molecular weight of ions ($g \cdot mol^{-1}$),n is the valence number of the ion (n = 1),F is the Faraday constant ($96485 C \cdot mol^{-1}$), I is the current (A) and t is the time (s). Furthermore, combining eqns. (1) and (4), the molecular weight ($M_w^{'}$) of the species that interacts with the electrode during the electrochemical process is calculated from the slope of the $\Delta m - Q$ curve by the following equation:

$$\frac{M_w^{'}}{nF} = \frac{m}{Q} \quad (5)$$

3. Results and discussion

Fig. 1(a) and (b) show high-resolution TEM images of the CDC-800 and CDC-1100 porous carbons, respectively. A typical microstructure consisting of highly curved graphene planes was observed for the CDC-800, with a few fullerenic shell-type structures present, indicating poor short-range local ordering. When the synthesis temperature is increased to 1100 ℃, straight graphite fringes with longer-range structural ordering are visible. This result is in agreement with previous reports showing that TiC-CDC powders prepared at higher temperatures have a more graphitized carbon microstructure [8,9]. Previous works based on XRD and Raman experiments have also shown that long-range carbon ordering (graphitization) occurs at 1100 ℃ [6,21]. The porosity of the two carbons was further analyzed by Ar adsorption and the corresponding isotherms are shown in Fig. 1(c). A typical type I gas isotherm was obtained for both of these carbons [22]. The calculated NL-DFT SSA of CDC-800 and CDC-1100 is 1479 $m^2 \cdot g^{-1}$ and 1526 $m^2 \cdot g^{-1}$, respectively. Although a slight hysteresis is present for the CDC-1100 sample, showing a small mesoporous volume, both CDC-800 and CDC-1100 have a similar narrow pore size distribution and an average pore size of about 1 nm (Table 1). The cumulative pore volume (CPV) distributions were calculated by summing individual pore volumes and are shown in Fig. 1 (d). As expected, both carbons have a similar CPV. More specifically, the porous volume for pore sizes below 1.1 nm was measured at 0.554 $cc \cdot g^{-1}$ and 0.397 $cc \cdot g^{-1}$, representing 79% and 63% of the total microporous volume of the CDC-800 and CDC-1100 carbons, respectively.

The electrochemical characterization of these two carbon electrodes was performed in a three-electrode cell in 2 M EMI-TFSI/ACN electrolyte. Fig. 2 presents the CVs of CDC-800 and CDC-1100 electrodes recorded at a scan rate of 5 $mV \cdot s^{-1}$, from − 1 V to + 1.5 V vs. Ag wire. Both electrodes show rectangular and symmetric CV plots characteristic of a capacitive charge storage mechanism (double-layer charge/discharge). The calculated gravimetric specific capacitance for CDC-800 and CDC-1100 electrodes is 100 $F \cdot g^{-1}$ and 75 $F \cdot g^{-1}$ at a scan rate of 5 $mV \cdot s^{-1}$, respectively. These values are similar to results obtained previously [9–11,23]. Our earlier results using CDC materials have shown that the microporous volume below 1.1 nm is responsible for the capacitive charge storage in CDC carbons [1,2,10,24–26]. This is confirmed by the present results, since the capacitance of the CDC-800 is 33% higher than that of CDC-1100, as the result of a 38% increase in the porous volume below 1.1 nm.

The potential of zero charge (PZC), that is, the potential where the electrode net surface charge is zero, was measured as the minimum capacitance on the CVs and further used as the origin of the charge ($Q = 0$ at the PZC) [27]. The PZC values for CDC-800 and CDC-1100 electrodes are about + 0.2 V vs. Ag and +0.4 V vs. Ag, respectively. Solid evidence from nuclear magnetic resonance experiments and molecular dynamics simulations has confirmed that CDC nanoporous carbon pores are filled with ions and solvent molecules when immersed in the electrolyte, even without any applied potential [13]. In the present situation, the more positive PZC value obtained for the CDC-1100 carbon suggests a more negative surface charge, which may result from specific interactions/adsorption between the anions and the carbon surface [16,28].

EQCM is a convenient tool for monitoring mass change at the nanogram scale during the electrochemical polarization of porous car-

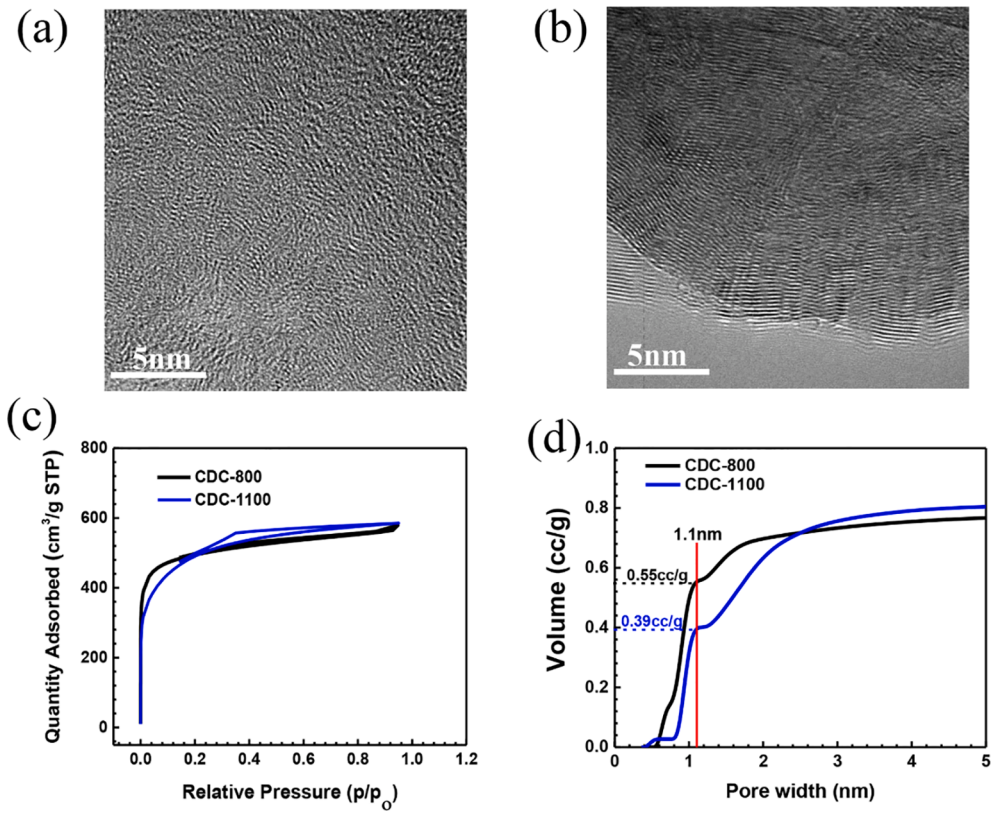

Fig. 1. High-resolution TEM images of TiC-CDC synthesized at (a) 800 °C and (b) 1100 °C. (c) Ar adsorption isotherm profile at 77 K and (d) cumulative pore volume distributions of TiC-CDC synthesized at (black line) 800 °C and (blue line) 1100 °C.

Table 1
CDC porosity measurements obtained using the Ar gas sorption technique.

Chlorination temperature (°C)	NL-DFT SSA ($m^2 \cdot g^{-1}$)	Microporous volume, <2 nm ($cc \cdot g^{-1}$)	Mesoporous volume ($cc \cdot g^{-1}$)	Total volume ($cc \cdot g^{-1}$)
800	1479	0.697	0.151	0.848
1100	1526	0.638	0.206	0.837

bon electrodes, providing direct information to help in identifying ion fluxes [26,28,29]. Fig. 3(a) and 3(b) show the CVs and EQCM responses of CDC-800 and CDC-1100 coated on the Au-quartz electrodes (see experimental section), in 2 M EMI-TFSI/ACN electrolyte at a scan rate of 10 $mV \cdot s^{-1}$, where the current and frequency changes are shown by the dashed and solid lines, respectively. Again, the CVs of both CDC-coated quartz electrodes exhibit a rectangular box shape, which is associated with capacitive behavior. For the CDC-800 sample, the frequency response (Δf) drastically decreases during both positive and negative polarization vs. the PZC, in a symmetrical way. The plot exhibits a near-flat zone within a potential range of 200 mV around the PZC. A decrease in Δf around the PZC was also observed for the CDC-1100 sample (Fig. 3b), with two main important differences: (i) the Δf flat zone was extended within a 0.7 V potential range (shaded region) compared to the CDC-800 sample and (ii) the Δf plot was not symmetric vs. the PZC.

The motional resistance change of CDC-800 and CDC-1100 coated Au electrodes during electrochemical charging/discharging is presented in Fig. 3(c) and (d). In both cases, the maximum change in motional resistance is less than 1/30th of the change in frequency, validating the gravimetric analysis of the EQCM data [30]. Moreover, the $-\Delta f$ vs. ΔR plots of the CDC-800 and CDC-1100 samples confirm the validity of the gravimetric approach (see Fig. S1 in the Supplementary Information) [31–34]. According to the Sauerbrey equation, a decrease in frequency will produce an increase in mass. Furthermore, the Δf for both carbon electrodes almost overlaps during the forward and reverse scans,

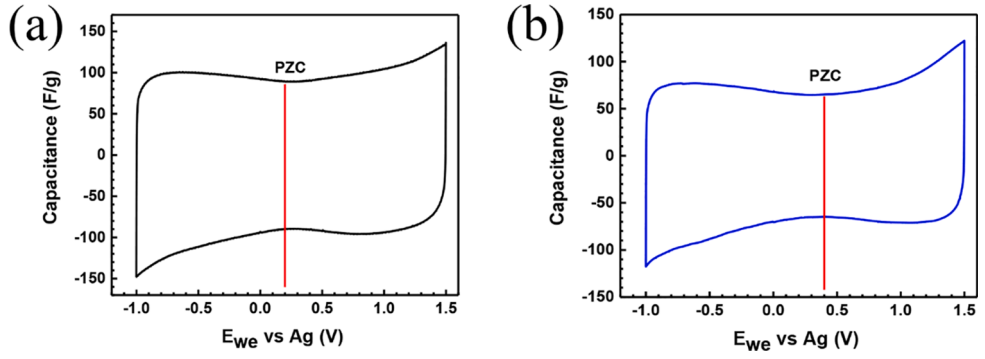

Fig. 2. CVs of (a) CDC-800 and (b) CDC-1100 film electrodes at a scan rate of 5 $mV \cdot s^{-1}$ in 2 M EMI-TFSI/ACN electrolyte.

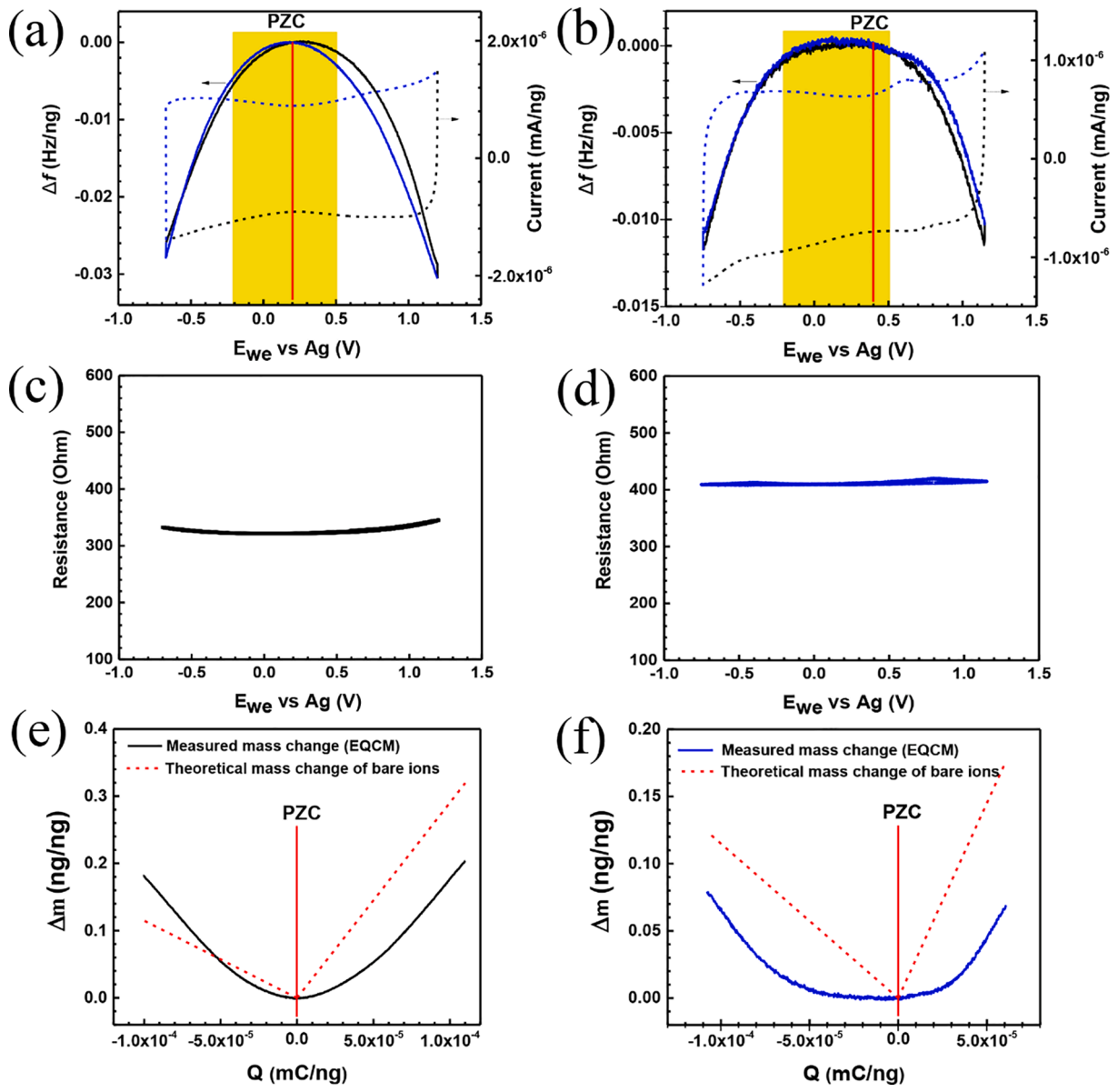

Fig. 3. CV and EQCM frequency response of (a) CDC-800- and (b) CDC-1100-coated Au electrodes in 2 M EMI-TFSI/ACN electrolyte at a scan rate of 10 mV·s^{-1}. The corresponding motional resistance change of (c) CDC-800 and (d) CDC-1100. Electrode mass change versus charge during the polarization of (e) CDC-800 and (f) CDC-1100.

indicating good reversibility of mass change.

The mass changes of the electrodes (Δm) were calculated using the Sauerbrey equation and plotted vs. the charge, with the PZC selected as the origin of the charge ($Q = 0$). As shown in Fig. 3(e), the mass of the CDC-800 electrode increased during both negative and positive polarization, corresponding to a charge storage mechanism by counter-ion adsorption,

where cations (anions) are adsorbed during negative (positive) polarization. The transition zone from cation to anion adsorption occurs within a narrow potential range around the PZC (200 mV), indicating a fast transition between the two processes. Overall, the relationship between Δm and Q for the CDC-800 electrode exhibits a 'V-shape' behavior, with a linear change on both sides of the PZC. A conventional counter-ion adsorption process was observed for the more graphitized CDC-1100 electrode.

At a high negative or positive polarization (Fig. 3f), the electrode weight change was different around the PZC. More specifically, the electrode weight change remained small and roughly constant within about 700 mV potential range during negative polarization; this is consistent with an ion-exchange charge storage mechanism, where $TFSI^-$ anions are desorbed (expelled) from the carbon surface while, at the same time, EMI^+ cations are adsorbed into the carbon pores. These results are consistent with an excess of $TFSI^-$ anions on the surface of the CDC-1100 nanopores at the open circuit potential, a result of the strong interaction between $TFSI^-$ anions and the carbon surface for the more graphitized CDC-1100 sample.

These results show the correlation between the PZC and the charge storage mechanism. An increase in the local graphitization of porous carbon results in stronger interactions between the $TFSI^-$ anions and the carbon surface in the pore, changing the PZC. As a result, a change in ion fluxes from counter ion adsorption (CDC-800 sample) to ion exchange process (CDC-1100 sample) was also observed. The increased carbon/anion interactions could be due to a more hydrophobic carbon surface produced by increased local graphitization, but additional experiments are needed to confirm the origin of this specific interaction.

4. Conclusion

EQCM was used to understand the charging mechanisms in TiC-CDC electrodes with different degrees of graphitization for capacitive charge storage applications (supercapacitors). Two CDC carbons were prepared by heat treatment of TiC powders under Cl_2 atmosphere at different temperatures: CDC-800 (800 °C synthesis temperature) and CDC-1100 (1100 °C temperature). Both carbons have a similar porous volume and pore size distribution, but the CDC-1100 prepared at the higher temperature (1100 ℃) has a more graphitized local carbon structure. The PZC of the CDC-1100 was found to be more positive (+0.4 V vs. Ag wire) than the CDC-800 (+0.2 V vs. Ag wire), suggesting the presence of a more negative charge on the carbon surface of the CDC-1100 sample at the OCV. Electrochemical results showed a dominant ion-exchange charge storage mechanism during negative polarization for the CDC-1100 sample, while the CDC-800 sample showed a symmetrical counter-ion charge storage process, as expected. A stronger interaction between the ions and the graphitized carbon surface is proposed to explain the above difference, which is supported by the PZC values of the two carbons. Such a difference in the ion fluxes connected to the change in the PZC value is important for the capacitive storage mechanism as it may affect the kinetics of the charge storage mechanism. These results are also important beyond the energy storage field in areas such as capacitive water desalination, as ion removal is maximized only during the counter ion adsorption process but not for the ion-exchange mechanism.

Declaration of Competing Interest

The authors declare that they have no known competing financial interests or personal relationships that could have appeared to influence the work reported in this paper.

Acknowledgements

HY was supported by a grant from the China Scholarship Council (no. 201806070153). PS, PLT, BD, HS and HY are grateful for support from the European Research Council (ERC) and Réseau sur le Stockage Electrochimique de l'Energie (RS2E).

Appendix A. Supplementary data

Supplementary data to this article can be found online at https://doi.org/10.1016/j.elecom.2022.107258.

References

[1] H. Shao, Y.C. Wu, Z. Lin, P.L. Taberna, P. Simon, Nanoporous carbon for electrochemical capacitive energy storage, Chem. Soc. Rev. 49 (10) (2020) 3005–3039.
[2] P. Simon, Y. Gogotsi, Perspectives for electrochemical capacitors and related devices, Nat. Mater. 19 (11) (2020) 1151–1163.
[3] Z. Lian, H. Chao, Z.G. Wang, Effects of confinement and ion adsorption in ionic liquid supercapacitors with nanoporous electrodes, ACS Nano 15 (7) (2021) 11724–11733.
[4] P.H. Huang, M. Heon, D. Pech, M. Brunet, P.L. Taberna, Y. Gogotsi, S. Lofland, J. D. Hettinger, P. Simon, Micro-supercapacitors from carbide derived carbon (CDC) films on silicon chips, J. Power Sources 225 (2013) 240–244.
[5] L.L. Zhang, X.S. Zhao, Carbon-based materials as supercapacitor electrodes, Chem. Soc. Rev. 38 (2009) 2520–2531.
[6] R. Dash, J. Chmiola, G. Yushin, Y. Gogotsi, G. Laudisio, J. Singer, J. Fischer, S. Kucheyev, Titanium carbide derived nanoporous carbon for energy-related applications, Carbon 44 (12) (2006) 2489–2497.
[7] M. Heon, S. Lofland, J. Applegate, R. Nolte, E. Cortes, J.D. Hettinger, P.L. Taberna, P. Simon, P. Huang, M. Brunet, Y. Gogotsi, Continuous carbide-derived carbon films with high volumetric capacitance, Energy Environ. Sci. 4 (1) (2011) 135–138.
[8] J. Chmiola, G. Yushin, R. Dash, Y. Gogotsi, Effect of pore size and surface area of carbide derived carbons on specific capacitance, J. Power Sources 158 (1) (2006) 765–772.
[9] C.R. Pérez, S.H. Yeon, J. Ségalini, V. Presser, P.L. Taberna, P. Simon, Y. Gogotsi, Structure and electrochemical performance of carbide-derived carbon nanopowders, Adv. Funct. Mater. 23 (8) (2013) 1081–1089.
[10] J. Chmiola, G. Yushin, Y. Gogotsi, C. Portet, P. Simon, P.L. Taberna, Anomalous increase in carbon capacitance at pore sizes less than 1 nanometer, Science 313 (5794) (2006) 1760–1763.
[11] C. Largeot, C. Portet, J. Chmiola, P.L. Taberna, Y. Gogotsi, P. Simon, Relation between the ion size and pore size for an electric double-layer capacitor, J. Am. Chem. Soc. 130 (9) (2008) 2730–2731.
[12] A.C. Forse, J.M. Griffin, C. Merlet, P.M. Bayley, H. Wang, P. Simon, C.P. Grey, NMR study of ion dynamics and charge storage in ionic liquid supercapacitors, J. Am. Chem. Soc. 137 (22) (2015) 7231–7242.
[13] A.C. Forse, C. Merlet, J.M. Griffin, C.P. Grey, New perspectives on the charging mechanisms of supercapacitors, J. Am. Chem. Soc. 138 (18) (2016) 5731–5744.
[14] J.M. Griffin, A.C. Forse, H. Wang, N.M. Trease, P.L. Taberna, P. Simon, C.P. Grey, Ion counting in supercapacitor electrodes using NMR spectroscopy, Faraday Discuss. 176 (2014) 49–68.
[15] J.L. Ye, Y.C. Wu, K. Xu, K. Ni, N. Shu, P.L. Taberna, Y.W. Zhu, P. Simon, Charge storage mechanisms of single-layer graphene in ionic liquid, J. Am. Chem. Soc. 141 (42) (2019) 16559–16563.
[16] Y.C. Wu, J.L. Ye, G. Jiang, K. Ni, N. Shu, P.L. Taberna, Y.W. Zhu, P. Simon, Electrochemical characterization of single layer graphene/electrolyte interface: Effect of solvent on the interfacial capacitance, Angew. Chem. Int. Ed. 60 (24) (2021) 13317–13322.
[17] Y. Cao, S. Li, C. Xu, X. Ma, G. Huang, C. Lu, Z. Li, Mechanisms of porous carbon-based supercapacitors, ChemNanoMat 7 (12) (2021) 1273–1290.
[18] C.D. Tomas, I.S. Martinez, F.V. Burgos, M.J. Lopez, K. Kaneko, N.A. Marks, Structural prediction of graphitization and porosity in carbide-derived carbons, Carbon 119 (2017) 1–9.
[19] Y. Gogotsi, A. Nikitin, H. Ye, W. Zhou, J.E. Fischer, B. Yi, H.C. Foley, M. W. Barsoum, Nanoporous carbide-derived carbon with tunable pore size, Nat. Mater. 2 (9) (2003) 591–594.
[20] G. Sauerbrey, The use of quarts oscillators for weighing thin layers and for microweighing, Z. Phys. 155 (1959) 206–222.
[21] I. Tallo, T. Thomberg, H. Kurig, A. Jänes, K. Kontturi, E. Lust, Supercapacitors based on carbide-derived carbons synthesised using HCl and Cl_2 as reactants, J. Solid State Electrochem. 17 (1) (2013) 19–28.
[22] M. Thommes, K. Kaneko, A.V. Neimark, J.P. Olivier, F.R. Reinoso, J. Rouquerol, K. S.W. Sing, Physisorption of gases, with special reference to the evaluation of surface area and pore size distribution (IUPAC Technical Report), Pure Appl. Chem. 87 (2015) 1051–1069.
[23] V. Presser, M. Heon, Y. Gogotsi, Carbide-derived carbons – from porous networks to nanotubes and graphene, Adv. Funct. Mater. 21 (5) (2011) 810–833.
[24] J. Chmiola, C. Largeot, P.L. Taberna, P. Simon, Y. Gogotsi, Desolvation of ions in subnanometer pores and its effect on capacitance and double-layer theory, Angew. Chem. Int. Ed. 120 (18) (2008) 3440–3443.
[25] N. Jäckel, P. Simon, Y. Gogotsi, V. Presser, Increase in capacitance by subnanometer pores in carbon, ACS Energy Lett. 1 (6) (2016) 1262–1265.
[26] M. Salanne, B. Rotenberg, K. Naoi, K. Kaneko, P.L. Taberna, C.P. Grey, B. Dunn, P. Simon, Efficient storage mechanisms for building better supercapacitors, Nat. Energy 1 (2016) 16070.
[27] M.T. Alam, M.M. Islam, T. Okajima, T. Ohsaka, Capacitance measurements in a series of room-temperature ionic liquids at glassy carbon and gold electrode interfaces, J. Phys. Chem. C 112 (42) (2008) 16600–16608.
[28] W.Y. Tsai, P.L. Taberna, P. Simon, Electrochemical quartz crystal microbalance (EQCM) study of ion dynamics in nanoporous carbons, J. Am. Chem. Soc. 136 (24) (2014) 8722–8728.
[29] M.D. Levi, G. Salitra, N. Levy, D. Aurbach, J. Maier, Application of a quartz-crystal microbalance to measure ionic fluxes in microporous carbons for energy storage, Nat. Mater. 8 (11) (2009) 872–875.
[30] P. Lemaire, T. Dargon, D. Alves Dalla Corte, O. Sel, H. Perrot, J.M. Tarascon, Making advanced electrogravimetry as an affordable analytical tool for battery interface characterization, Anal. Chem. 92 (20) (2020) 13803–13812.
[31] H. Muramatsu, E. Tamiya, I. Karube, Computation of equivalent circuit parameters of quartz crystals in contact with liquids and study of liquid properties, Anal. Chem. 60 (19) (1988) 2142–2146.
[32] H. Muramatsu, X. Ye, M. Suda, T. Sakuhara, T. Ataka, In-situ monitoring of microrheology on electrochemical deposition using an advanced quartz crystal analyzer and its application to polypyrrole deposition, J. Electroanal. Chem. 322 (1-2) (1992) 311–323.
[33] H. Muramatsu, J. Kim, S. Chang, Quartz-crystal sensors for biosensing and chemical analysis, Anal. Bioanal. Chem. 372 (2) (2002) 314–321.
[34] X.L. Su, Y. Li, A QCM immunosensor for salmonella detection with simultaneous measurements of resonant frequency and motional resistance, Biosens. Bioelectron. 21 (6) (2005) 840–848.